In situ engineering of an ultrathin polyamphoteric layer on polyketone-based thin film composite forward osmosis membrane for comprehensive anti-fouling performance

Lei Zhang[a,b1], Ralph Rolly Gonzales[b,c1], Titik Istirokhatun[b,e], Yuqing Lin[b], Jumpei Segawa[b,d], Ho Kyong Shon[c], Hideto Matsuyama[b,d]*

[a] *School of Chemistry and Chemical Engineering, Shandong University of Technology, Zibo, China*

[b] *Research Center for Membrane and Film Technology, Kobe University, Kobe, Japan*

[c] *Centre of Technology in Water and Wastewater, University of Technology Sydney, New South Wales, Australia*

[d] *Department of Chemical Science and Engineering, Kobe University, Kobe, Japan*

[e] *Department of Environmental Engineering, Faculty of Engineering, Diponegoro University, Jl. Prof. Soedarto-Tembalang, Semarang, Indonesia*

[*] Corresponding author: E-mail*:* matuyama@kobe-u.ac.jp

[1] These authors contributed equally to this work.

Abstract:

Thin film composite (TFC) membranes easily suffer from fouling induced by oil and other pollutants during forward osmosis (FO) due to the relatively hydrophobic chemistry and rough structure of polyamide (PA). To achieve comprehensive anti-fouling properties, poly(2-methacryloyloxyethyl phosphorylcholine-co-2-aminoethyl methacrylate hydrochloride) (MPC-co-AEMA) was immobilized on top of a polyketone (PK)-based TFC membrane following a single-step simultaneous deposition with dopamine. The adhesive properties of polydopamine (PDA), as well as the covalent interactions between PDA and MPC-co-AEMA, ensured the firm immobilization of the MPC-co-AEMA on PA layer. As a result of the simultaneous deposition of PDA and MPC-co-AEMA, a high-performance and superhydrophilic and underwater superoleophobic TFC membrane was engineered. In addition, the outstanding water adsorption capacity of the polyamphoteric layer resulted in better protein adhesion mitigation. FO operation using various foulants also demonstrated a high fouling resistance of the PK-TFC-PDA/MPC membrane, especially during the treatment of wastewater emulsion containing high concentration of oil and bovine serum albumin (BSA). In summary, the findings in this study could provide insights into the preparation of anti-fouling membranes for wastewater purification using FO.

Keywords: Forward osmosis; Thin film composite membrane; Polydopamine; Polyamphoteric; Anti-fouling

1. Introduction

With the rapid industrialization development and population growth, a vast amount of wastewater (e.g. oily wastewater) is produced, posing a hazard to the ecosystem and human health [1]. Proper management and treatment of problematic wastewater have become big challenges worldwide. Membrane separation is among the most promising technologies for water treatment and purification due to its simplicity and high separation efficiency [2, 3]. In comparison with other pressure-driven membrane separation processes, e.g., reverse osmosis (RO) and nanofiltration (NF), osmosis-driven forward osmosis (FO) has the advantages of higher recovery, lower energy consumption, and reduced fouling capability [4-6]. An integral focus in FO research is the manufacture of thin-film composite (TFC) membrane, typically composed of a porous support and a thin polyamide (PA) active layer [7]. The asymmetric structure of TFC membranes allows it to be used for two orientations during FO operation: active layer on the feed stream side (AL-FS, or FO mode) and active layer on the draw stream side (AL-DS, or PRO mode). The membrane orientation during FO operation influences the process and membrane performance. Typically, FO membranes operated in AL-DS mode have higher water permeability because of internal concentration polarization (ICP) retardation [8]; however, this membrane orientation makes the membrane support layer more susceptible to fouling, as the foulant particles can easily go through the membrane support's porous structure and block the pores [9]. One of the biggest issues to be addressed in development of FO membranes is the occurrence of membrane fouling. Membrane fouling has become a severe bottleneck in development of large-scale FO system operations, since membrane fouling negatively affects membrane performance, resulting in increased operation costs. Despite the lower propensity of membrane fouling at AL-FS operation, the slightly hydrophobic nature and rough structure of the PA active layer could still result in membrane fouling

[4]. Thus, the fabrication of TFC membrane with high fouling-resistance for water purification in FO system, regardless of membrane orientation, is still desired.

Engineering a layer with high water adsorption capacity on the membrane surface using a hydrophilic material is among the most efficient strategies to inhibit membrane fouling by preventing the contact between the membrane and foulants [10, 11]. Among previously reported hydrophilic materials in literature, polyamphoteric polyelectrolytes, or substances endowed with equal amounts of positively- and negatively-charged functional groups, exhibit remarkably low fouling potential to a variety of foulants, because of the strong water adsorption capacity arising from electrostatic interactions between the water molecules and charged moities [12-14]. The polyamphoteric materials, also known as zwitterions, can be used for membrane modification by blending [15], surface grafting [16], and surface coating [17]. For instance, Liu et al. immobilized zwitterionic polymers on TFC membrane by atom-transfer radical-polymerization (ATRP) method [18]. The obtained membrane showed high anti-fouling performance compared with the pristine TFC and silica-decorated TFC membranes when sodium alginate was used as foulant in the FO fouling experiment. The pristine TFC membrane showed 24% water flux decline, and after modification, water flux decline reduced to 10%. Furthermore, number of attached live *E. coli* bacteria on the membrane surface was also significantly reduced after modification. Zhang et al. grafted polyamphoteric poly(sulfobetaine mathacrylate) (PSBMA) brushes on commercial FO TFC membrane surface via ATRP [19]. Fouling experiments using oil-water emulsion feed solution were performed. The TFC-PSBMA exhibited better flux recovery (30% decline) compared with the pristine TFC membrane (56% decline). FO membrane with dual skin layers: a polyamide layer and a PSBMA-decorated multi-walled carbon nanotube (MWCNT/PSBMA) fouling-resistant layer was prepared in a follow-up study [20]. Using protein and carbohydrate model foulants, the water flux recovery values of the MWCNT/PSBMA-modified TFC

membrane were observed to be 85% and 82%, respectively, vastly improving from the fouling effect on the water flux of pristine TFC membranes. However, these modification methods are difficult for large-scale application because of the complex processes (i.e., surface initiation and zwitterionic monomer polymerization) and severe condition (i.e., N_2 atmosphere). For the blending and coating strategies, stability of the modification layer is still a big problem for long-term operation in water purification [21]. Therefore, simple and efficient methods for immobilization of polyamphoteric molecules on TFC membrane surface remains to be explored.

Recently, dopamine adhesion has attracted attention for membrane surface modification, among other applications [22-24]. The self-polymerization of dopamine into polydopamine (PDA) in alkaline environment, which can be easily adhered on almost any surface in neutral or base environment due to the covalent bonding of catechol and amine structures [25]. Also, PDA can be used in immobilization of certain molecules on most surfaces via simultaneous deposition [26-28]. Furthermore, PDA is also known to interact with amines and thiols through Michael addition or oxidative Schiff base reactions [29]. Using this knowledge regarding the properties of PDA, we expect that immobilization of amine-containing polyamphoteric materials is possible on the TFC membrane surface via a single-step covalent cross-linking and simultaneous deposition with dopamine.

In this work, a newly synthesized amine-containing polyamphoteric material, poly(2-methacryloyloxyethyl phosphorylcholine-co-2-aminoethyl methacrylate hydrochloride) (MPC-co-AEMA), was used to modify the TFC membrane via single-step simultaneous deposition with polydopamine. The surface morphology, chemical composition, and wettability of the PK support and TFC membranes were systematically evaluated by SEM, XPS, and contact angle measurement. Due to the presence of a strong hydration layer, a barrier against oil and protein foulants was hypothesized to be formed in situ on the PK-TFC membrane surface and the modified PK-TFC-PDA/MPC

membrane would show comprehensive anti-fouling properties for the oil-water emulsion and protein molecules during FO process.

2. Experimental

2.1. Reagents

Aliphatic polyketone (200,000 g mol^{-1}, Asahi Kasei Co., Ltd., Japan), was the chosen support polymer material. Resorcinol (>99.0%), methanol (>99.8%), acetone (>99.8%), and hexane (>99.8%), used for membrane support preparation, were procured from Fujifilm Wako Pure Chemical Corp. (Japan). Trimesoyl chloride (TMC), *m*-phenylenediamine (MPD), sodium dodecyl sulfonate (SDS), triethylamine (TEA), and 10-camphorsulfonic acid (CSA), obtained from Wako Pure Chemical Co. (Japan), were used for interfacial polymerization. Membrane modification was carried out with dopamine (DA, Sigma-Aldrich, Japan) and 25% NH_3 solution (Fujifilm Wako Pure Chemical Corp., Japan). Poly(2-methacryloyloxyethyl phosphorylcholine-co-2-aminoethyl methacrylate hydrochloride) (MPC-co-AEMA copolymer, MPC: AEMA = 9:1 (mol/mol), 10% w/w solution, NOF Corp., Japan), whose structure is shown in Scheme 1, was used as the polyamphoteric material. For FO testing and membrane fouling studies, sodium chloride (NaCl, Wako Pure Chemical Co., Japan), soybean oil (Wako Pure Chemical Co., Japan), and bovine serum albumin (BSA, Sigma-Aldrich, Japan) were used as the draw solute and foulants. Chloroform (Wako Pure Chemical Co., Japan) was used for determination of membrane wettability. Fluorescently-labelled protein, albumin-fluorescein isothiocyanate conjugate (BSA-FITC, Sigma-Aldrich, Japan), was used and mixed in a pH 7.4 phosphate buffered saline (PBS) solution for protein adsorption studies. Milli-Q water produced in the laboratory was used in all experiments.

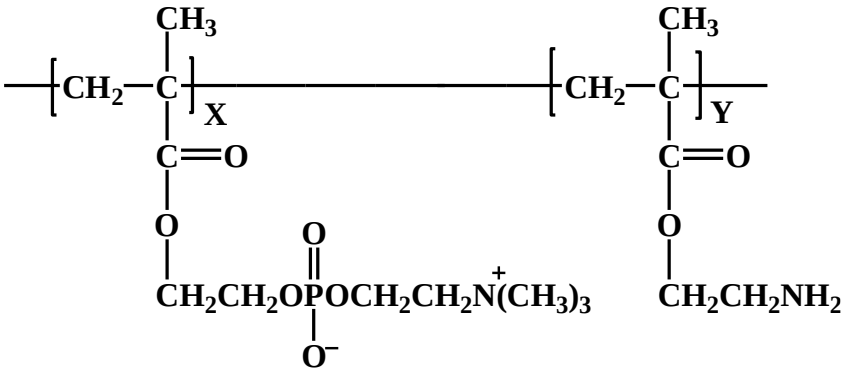

Scheme 1. Chemical structure of MPC-co-AEMA (X:Y=9:1)

2.2. Membrane preparation and modification

Flat-sheet PK support was fabricated by the conventional non-solvent induced phase separation (NIPS) method [30]. PK powder was dissolved in a 65% w/w aqueous resorcinol solution to create a 10% w/w PK solution, and the solution was constantly stirred at 80 °C for 5 h, or until homogeneous. The PK solution was afterwards kept in oven at 50°C for 24 h for degassing. After which, the solution was casted on a glass plate (casting thickness: 400 μm). The as-cast PK film was immediately immersed into a 35% w/w aqueous methanol coagulation bath maintained at ~25 °C for 20 min, followed by successive immersion for 20 min into acetone and hexane. Finally, the membrane was dried in the air, and named as PK support.

The fabrication method of PK-based TFC membrane is the same as our previous reported method [20]. The aqueous MPD solution was prepared to consist of 2.0% MPD, 1.1% TEA, 0.15% SDS, and 2.3% CSA (all w/w). The organic TMC solution consisted of 0.15 wt% TMC in hexane. Both of the solutions were stirred for at least 30 min to achieve homogeneity. The PK support was first fixed in an acrylic frame, and the MPD solution was poured on top. After 5 min, the remaining MPD solution was discarded and completely removed using an air knife. Then, the TMC solution was poured on the support. After 2 min, the remaining TMC solution was discarded and the TFC membrane was kept in air for 1 min to allow hexane evaporation. After that, the membrane was put into an oven at 90 °C for

10 min for cross-linkage. Lastly, the TFC membrane was rinsed with Milli-Q water for removal of unreacted monomers and stored in Milli-Q water prior to use. The obtained composite membrane was named as PK-TFC.

The MPC-co-AEMA polyamphoteric polymer was immobilized on the PK-TFC membrane surface via single-step simultaneous deposition with DA, as shown in Fig. 1(a) [31]. A solution containing 0.5 g DA, 10 g MPC-co-AEMA, 8 mL 25% ammonia solution, and 100 mL Milli-Q water was prepared. The PK-TFC membrane was then immersed into the DA/MPC-co-AEMA mixture for 9 h with slight shaking. The modified TFC membrane was rinsed with copious amounts of Milli-Q water and named PK-TFC-PDA/MPC.

2.3. Membrane characterization

Membrane surface morphology was observed by field-emission scanning electron microscopy (FE-SEM; JSF-7500F, JEOL, Tokyo, Japan). The polyamide layer thickness of the PK-TFC and PK-TFC-PDA/MPC membranes was evaluated using field emission transmission electron microscopy (FE-TEM; JEM-2100F, JEOL, Tokyo, Japan), with accelerating voltage of 200 kV [1]. Chemical composition was analyzed by the X-ray photoelectron spectroscopy (XPS; JPS-9010 MC, JEOL) with Al Kα X-rays. Surface wettability was evaluated by a contact angle measurement device (Drop Master, Kyowa Interface Science Co., Japan). Water contact angle and underwater chloroform contact angle were determined after placing a 4 μL droplet of water and chloroform, respectively, on the membrane surface. Membrane surface roughness was evaluated using a 3D laser scanning microscope (LSM; VK-X3000, Keyence Corp., Japan) with a scanning area of 135 μm x 135 μm. Dynamic chloroform adhesion experiment was also conducted by placing a 4 μL chloroform droplet on the membrane surface, followed by compression and detachment [32]. Static organic foulant adhesion was evaluated

using BSA-FITC [33]. The membrane sample was immersed in PBS containing 20 ppm fluorescently-labelled protein, placed in dark, agitating conditions for 12 h at room temperature. The sample was afterwards washed with PBS to rinse off loosely attached protein, before imaging with confocal laser scanning microscope (CLSM; FV1000D, Olympus, Japan).

2.4. TFC membrane intrinsic transport properties and FO performance evaluation

The intrinsic transport properties were evaluated using a bench-scale RO cross-flow system, whose effective membrane area is 8.07 cm^2 [34]. Pure water permeability (A, L m^{-2} h^{-1} bar^{-1}) was measured under an applied hydraulic pressure of 10 bar and flow rate of 9.9 mL min^{-1} and calculated based on Eq. (1):

$$A = \frac{V}{S \times t \times \Delta P} \quad (1)$$

where *V, S, t, and* ΔP are permeate volume (L), membrane area (m^2), time (h), and hydraulic pressure (bar), respectively [35].

Salt rejection (R) was measured using 2000 mg L^{-1} NaCl solution as feed under the same RO operation conditions and calculated based on Eq. (2):

$$R = \frac{(C_f - C_P)}{C_f} \times 100\% \quad (2)$$

where C_f and C_p are the respective feed and permeate NaCl concentrations, determined using a multimeter (B-771, Horiba, Japan).

After determination of A and R, salt permeability coefficient (B, L·m^{-2} h^{-1}) can be obtained using Eq (3):

$$B = \frac{(100-R) \times A \times (\Delta P - \Delta\pi)}{R} \quad (3)$$

where $\Delta\pi$ is 0.85, or the osmotic pressure of 2000 mg L^{-1} NaCl [36, 37].

Osmotic performance of the TFC membranes under FO operation was evaluated in AL-FS mode

by a bench-scale cross-flow system, whose effective membrane area is 2.54 cm^2. The feed and draw solutions (Milli-Q water and 1 M NaCl, respectively) were circulated by two gear pumps at a flow rate of 0.3 L/min. The mass changes of the feed solution were recorded by a top-loading balance. The water flux (J_w, $L\ m^{-2}\ h^{-1}$) and the reverse salt flux (J_s, g m^{-2} h^{-1}) were calculated by Eqs (4) and (5):

$$J_w = \frac{V}{S \times t} \quad (4)$$

$$J_s = \frac{\Delta(C_t \times V_t)}{S \times t} \quad (5)$$

where V, t, S, C_t, and V_t are volume change (L), time (h), effective area (m^{-2}), feed solution salt concentration, and feed volume, respectively [38, 39].

Using the solute diffusion coefficient D, the TFC membrane structure parameter (S, μm) was calculated by Eq. (6):

$$J_w = \frac{D}{S} \ln \frac{A \times \pi_D + B}{A \times \pi_F + J_w + B} \quad (6)$$

where π_D and π_F represent the respective osmotic pressures of the draw and feed solutions [40, 41].

3. Results and discussion

3.1. Membrane morphology

Fig. 1(a) shows the simultaneous deposition of DA and MPC-co-AEMA on the surface of PK-TFC membrane. The polyamphoteric MPC-co-AEMA contains amine groups which react via Michael-addition and oxidative Schiff-base interactions with PDA, resulting in formation of amine-functionalized aggregates which deposit onto the PA surface rapidly. The PDA and MPC-co-AEMA coating are then immobilized on the PA surface due to H-bonding and π-π interactions [31, 42]. The color change seen from Fig. 1(b) was caused by the simultaneous deposition of PDA and MPC-co-AEMA on the TFC membrane.

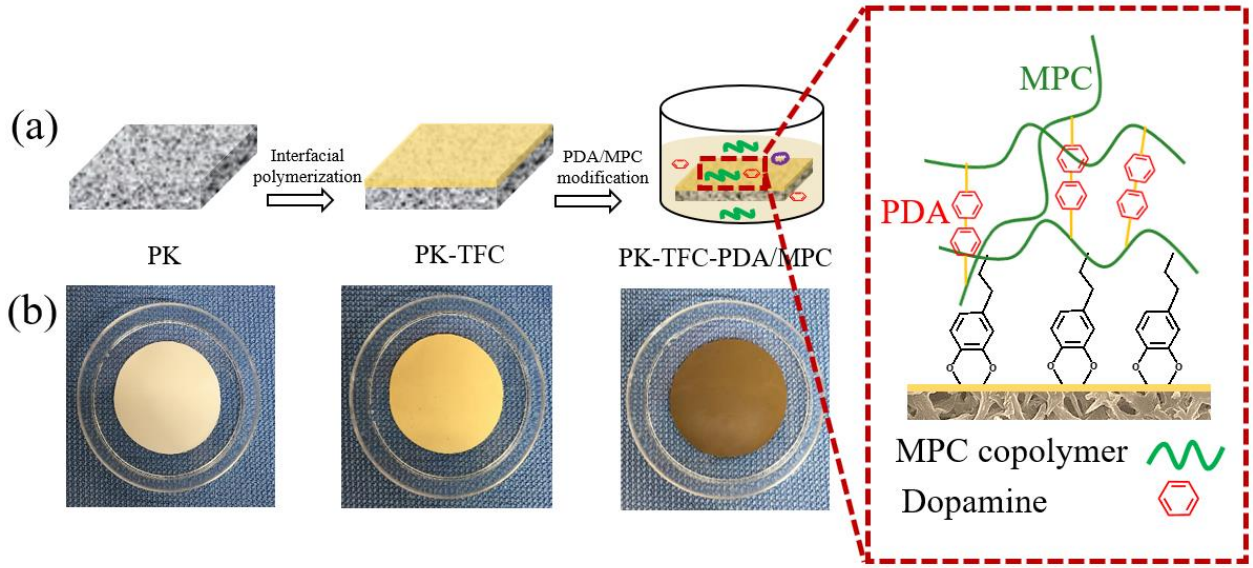

Fig. 1. (a) In situ polyamphoteric layer deposition on PK-based TFC membrane via simultaneous deposition with DA; (b) appearances of the PK support, PK-TFC, and PK-TFC-PDA/MPC.

The membrane morphology was characterized by FE-SEM (Fig. 2(a)-(d)). In Fig. 2(a)-(b). the PK support exhibited a porous fibril-like structure, which was similar with our previous results [43]. However, the PK-TFC membrane exhibited a dense surface with the ridge-and-valley structure typically observed for PA layer [44]. After simultaneous deposition of PDA and MPC-co-AEMA, the smoother PDA/MPC-co-AEMA layer surface could be seen at higher magnification. The cross-section structure of the PK support and TFC membranes was shown in Fig. 2(c)-(d). The PK support exhibited a fibrous structure without an obvious dense skin layer. However, a dense PA layer with an apparent thickness of 260 nm could be obviously observed on the PK support after interfacial polymerization. It should be noted that the real thickness of PA layer might be about 150 nm, which was far less than the apparent thickness. The crumpled morphology (ridge-and-valley structure) of the PA active layer causes an uneven layer on top of the membrane support layer, which appears to bend and crumple up in certain parts. The presence of the whole crumpled zone results in difference of apparent thickness

from actual thickness of the entire polyamide layer [45]. After the simultaneous deposition of PDA and MPC-co-AEMA, a similar PA layer (280 nm) was observed of the PK-TFC-PDA/MPC membrane. FE-TEM analysis was also performed to measure the thickness of the polyamide layer of PK-TFC and PK-TFC-PDA/MPC. As shown in Fig. 2(e), PK-TFC membrane was observed to have a polyamide thickness of 184 nm, while PK-TFC/PDA/MPC membrane showed a polyamide thickness of 197 nm. Both FE-SEM and TEM analyses demonstrated that the co-deposition with DA could form an ultrathin polyamphoteric layer on the PK-TFC membrane. The surface roughness of the membrane samples was determined by LSM analysis and the results are shown in Fig. 2(f). The PK membrane surface, which exhibited the hierarchical micro-/nanofibril-like structure [31], has an average arithmetical mean height (S_a) of 47.4 nm. After formation of the polyamide active layer during IP, membrane surface roughness increased to a S_a value of 92.8 nm, which corresponds to the crumpled morphology of the polyamide. After the one-step modification with PDA and MPC-co-AEMA, the PK-TFC-PDA/MPC membrane exhibited a S_a value of 40.0 nm.

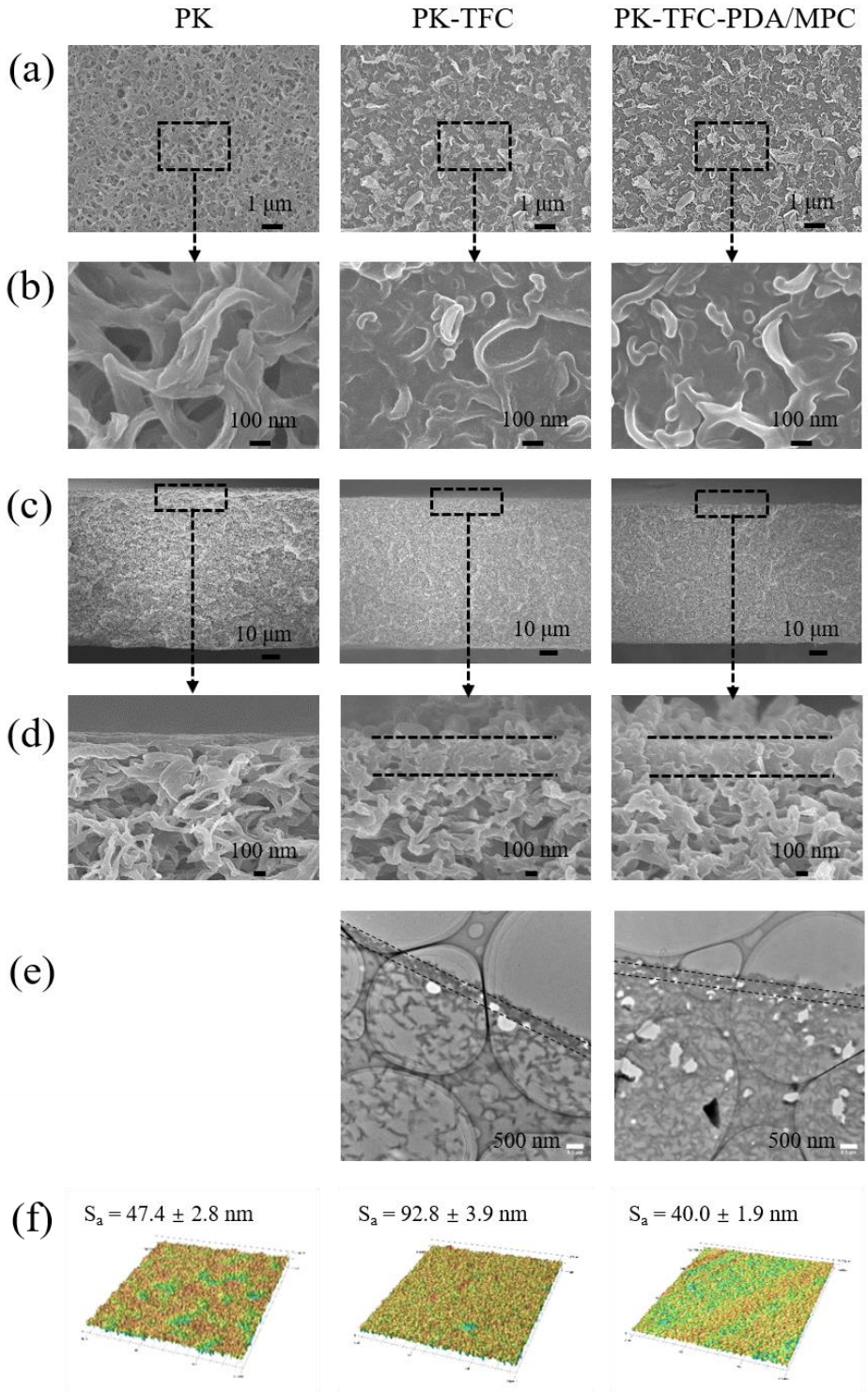

Fig. 2. (a)-(b) Surface and (c)-(d) cross-section morphologies of PK support, PK-TFC and PK-TFC-PDA/MPC membranes taken using FE-SEM analysis; (e) cross-section morphologies of PK-TFC and PK-TFC-PDA/MPC membranes taken using FE-TEM analysis; (f) membrane surface roughness taken using LSM analysis.

3.2. Membrane surface chemical composition

XPS characterization of the PK support and TFC membranes was performed to determine surface chemical composition (Table 1 and Fig. 3). Fig. 3(a) shows the presence of only two peaks corresponding to O (23.4%) and C (76.6%) for the PK support. As a result of the interfacial polymerization, N, originating from the PA layer, was observed on the PK-TFC membrane spectrum (13.5%). PA cross-linkage can be evaluated through the O/N ratio, such that when the O/N ratio is 1.0, the PA layer is known to be fully cross-linked. Full cross-linkage indicates that all the O and N atoms in the membrane surface were only from the PA amide groups, giving a 1:1 ratio [46]. Therefore, it was demonstrated that the PA active layer of PK-TFC membrane possessed a high cross-linking degree because of its similar O/N ratio of 0.97. A high degree of cross-linking of PA layer could enhance ion selectivity and eliminate water permeability hindrance [47]. However, the O/N ratio increased to 2.8 (exceeded the critical value of 2) after simultaneous deposition of MPC-co-AEMA and DA. This indicated that an O-rich material layer was covered on the PA layer. Furthermore, P (3.4%) was also measured, further confirming that the polyamphoteric layer was successfully deposited on the PK-TFC membrane surface.

Higher resolution scanning using XPS shows the C1s spectra for PK support, PK-TFC and PK-TFC-PDA/MPC membranes, as shown in Fig. 3(b)-(d). Multi-peak fitting was performed to analyze the chemical bonds associated with C1s. For the PK support, the C1s spectrum could be divided into a major peak at 286.2 eV (C-C/C-H) and a minor peak at 288.9 eV (C=O), corresponding to the carbon chain and the carbonyl group, respectively [48]. It was observed from Fig. 3(c) that the C1s spectrum of PK-TFC membranes was divided into three peaks, which ascribed to the N-C=O/O-C=O at 288.0 eV, C-N at 286.1 eV, and C–C/C–H at 284.5 eV, respectively[49]. It was interesting to found that the peak intensity of amide (N-C=O) and carboxylic (O-C=O) group disappeared for the PK-TFC-

PDA/MPC membrane, demonstrating that the PA layer was covered by other materials. The peaks at 287.3 eV (C=O) and 286.2 eV (C-N) could be attributed to the carbonyl and amine groups of both PDA and MPC-co-AEMA [50].

Table 1. Elemental composition of PK support and TFC membranes.

Membranes	C	O	N	P	O/N
PK	76.6	23.4	0	0	-
PK-TFC	75.4	13.1	13.5	0	0.97
PK-TFC -PDA/MPC	69.7	19.8	7.1	3.4	2.80

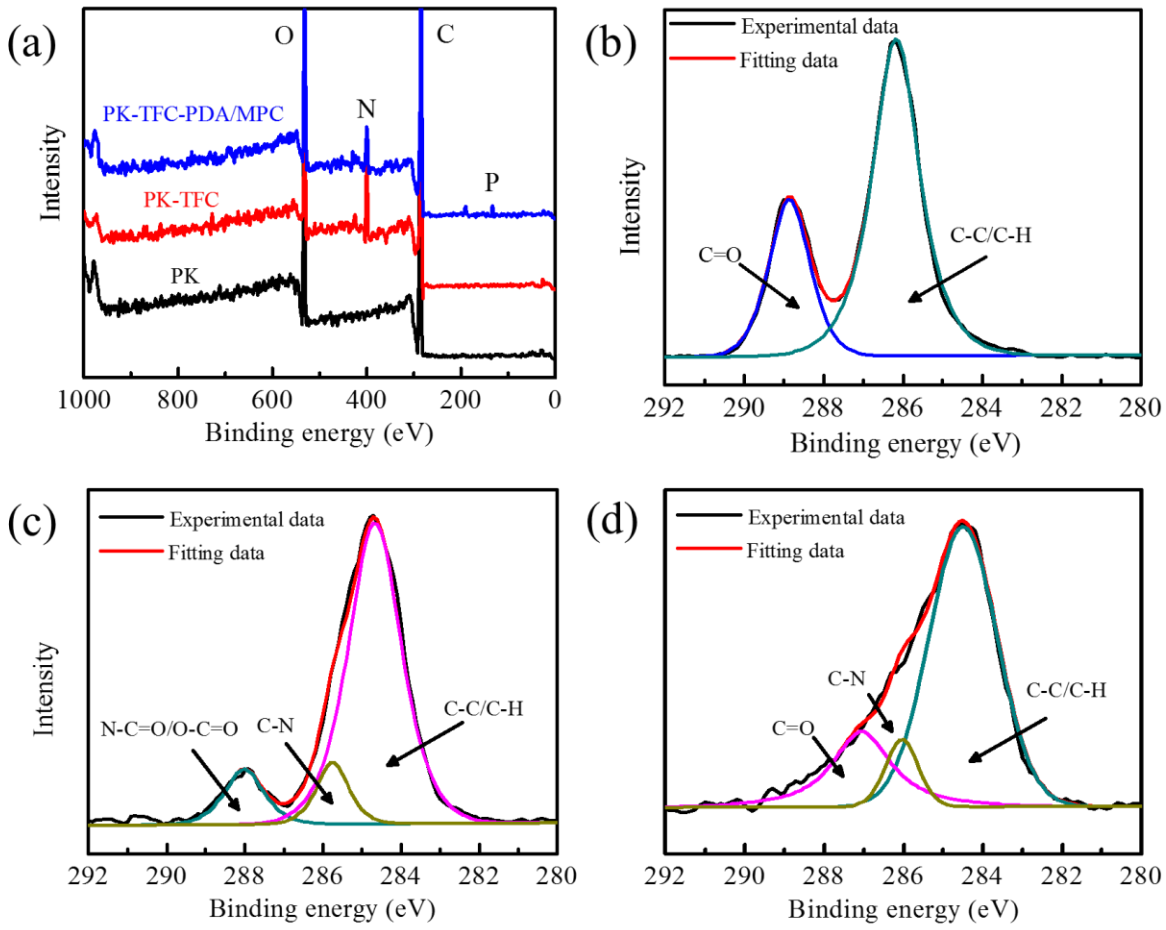

Fig. 3. (a) XPS surface chemical composition of the PK support and TFC membranes; (b)-(d) C1s spectrum of PK support, PK-TFC, and PK-TFC-PDA/MPC membranes.

3.3. Surface wettability and anti-oil-adhesion properties

Fig. 4 shows the surface wettability of the PK support and the TFC membranes. The water contact angle of PK support was 35°. After interfacial polymerization, the PK-TFC membrane water contact angle was found to be 56°, indicating the relatively hydrophobic property of the PA active layer. However, the PK-TFC-PDA/MPC membrane showed the lowest water contact angle of 7°, exhibiting a robust superhydrophilicity. The observed hydrophilicity of PK-TFC-PDA/MPC membrane was mainly caused by MPC-co-AEMA's strong water adsorption capacity, which leads to the water droplet to easily be absorbed and spread on the membrane surface [51]. Aside from hydrophilicity, surface wettability is also influenced by the roughness. The effect of surface roughness is given by the Wenzel equation (Eq. 7):

$$\cos\theta_{app} = r\cos\theta \quad (7)$$

where θ_{app}, θ, and r are the apparent contact angle, intrinsic contact angle (on a perfectly smooth solid surface), and the ratio of the real surface area of rough area and geometric projected area, respectively [52, 53]. Following the membrane surface roughness analysis results, as shown in Fig. 2(e), the membrane contact angles reported in this study are more highly influenced by the membrane chemical functionality. Despite the highest roughness exhibited by the PK-TFC membrane, it exhibited the highest contact angle (least hydrophobicity), indicating the relatively higher intrinsic hydrophobicity of the polyamide functional groups present on the active layer surface. After membrane modification, the contact angle of PK-TFC-PDA/MPC decreased significantly, despite having similar surface roughness with the PK substrate, indicating the presence of several hydrophilic functional groups introduced by both PDA and the MPC-co-AEMA.

The oil wettability of the membranes is shown in Fig. 4(b) from the underwater chloroform contact angles of PK support and TFC membranes. The chloroform contact of PK support was 27°,

indicating it could easily be wetted by chloroform, similar to our previous results [54]. The water in PK matrix was easily replaced by chloroform since the interaction between water and PK support was low. The PK-TFC membrane, on the other hand, exhibited a high underwater chloroform contact of 158°, attributed to the rough PA morphology and hydrophilicity of the carboxyl and amide groups. After simultaneous PDA and MPC-co-AEMA deposition, the PK-TFC-PDA/MPC membrane showed a similar high underwater chloroform contact angle. Furthermore, the dynamic approach-compression-detachment contact angle experiment was also conducted for evaluation of the anti-oil adhesion properties of both TFC membranes. Fig. 4(c) shows that the chloroform droplet could hardly be detached from the PK-TFC membrane surface, demonstrating high adhesion force. However, for the PK-TFC-PDA/MPC membrane, the chloroform droplet was easily detached from the membrane surface. It indicated that there was a low adhesion force between the membrane surface and chloroform. This is because the polyamphoteric MPC layer has strong water adsorption capacity and can therefore capture a thick water layer on membrane surface to prevent the adhesion of organic solvent or oil droplet on membrane surface [55]. The low adhesion force between the membrane surface and organic solvent droplet would promise a high anti-oil-fouling performance during the oil/water separation process.

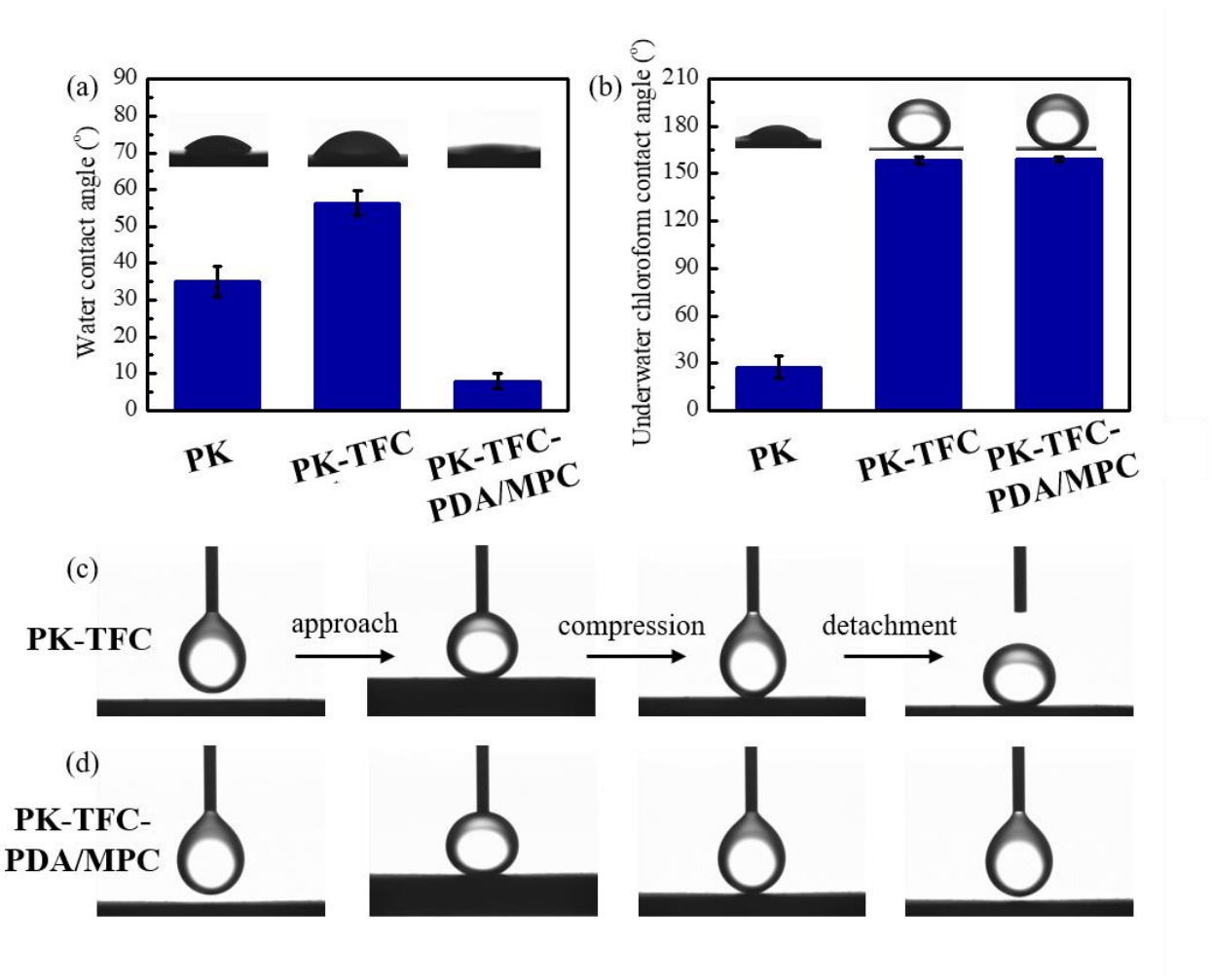

Fig. 4. (a) Water contact angle and (b) underwater chloroform contact angle of the PK support and TFC membranes; (c)-(d) anti-chloroform-adhesion properties of PK-TFC and PK-TFC-PDA/MPC membranes.

3.4. Anti-protein-adhesion properties

The anti-protein-adhesion ability of the PK support, PK-TFC, and PK-TFC-PDA/MPC membranes were investigated using BSA-FITC adsorption measurements. Fig. 5(a) shows the membrane images following fluorescent protein adsorption. ImageJ software was used to analyze the fluorescence intensity, and results are shown in Fig. 5(b). The PK support showed a mostly bright green image, corresponding to a fluorescence intensity of 86%, reflecting that the PK support was

severely fouled by BSA. After interfacial polymerization, the fluorescence intensity of PK-TFC membrane reduced to 43%. This might be due to the increased hydrophilicity of carboxyl group, compared to that of the carbonyl group. Besides, the electrostatic repulsion between PK-TFC membrane surface (isoelectric point at pH 4.7 [56]) and BSA molecule, both negatively-charged at pH ~7, also contributed to the low fluorescence intensity [57]. As expected, the fluorescence image of PK-TFC-PDA/MPC membrane was black with the lowest fluorescence intensity of 21%, indicating a robust anti-protein-adhesion property. The outstanding BSA adsorption mitigation of PK-TFC-PDA/MPC membrane was mainly a result of the water adsorption capacity of the polyamphoteric layer, which prevents the adhesion of BSA on membrane surface.

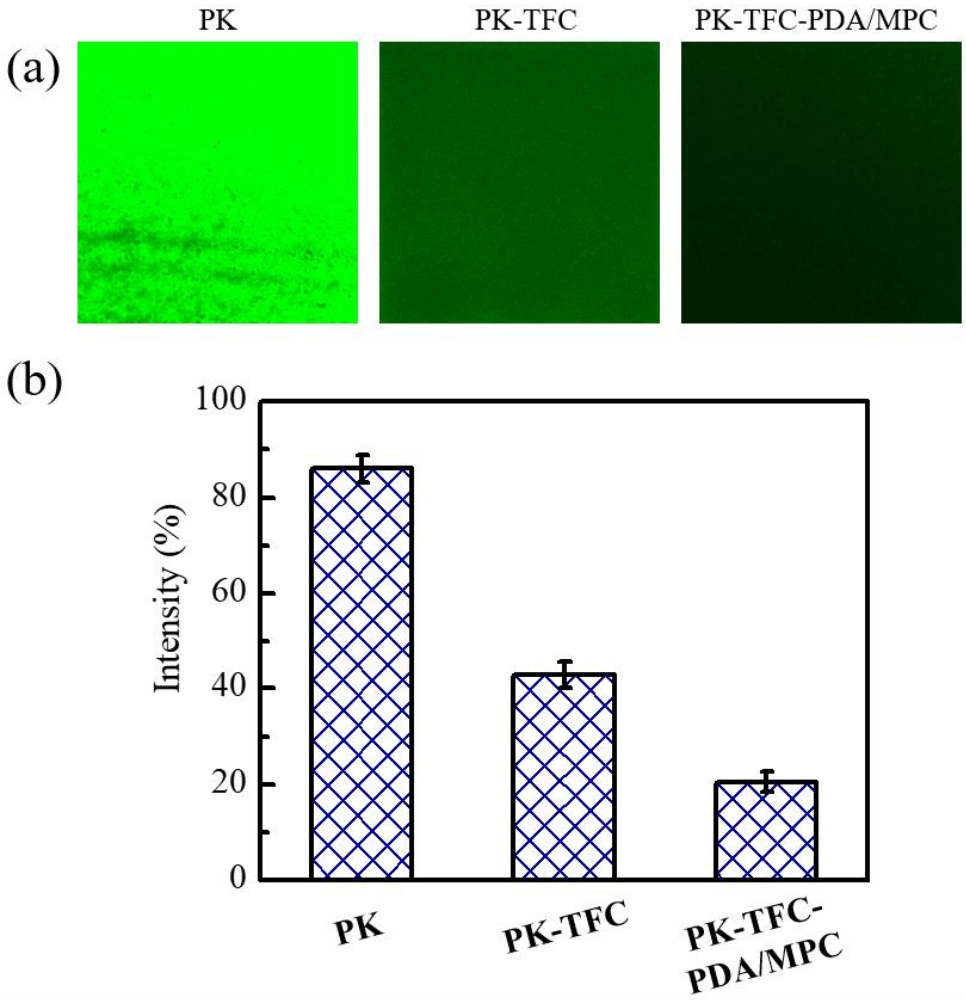

Fig. 5. (a) CLSM images and (b) fluorescence intensity of the PK support and TFC membranes.

3.5. TFC membrane intrinsic transport and anti-fouling properties

Before evaluation of osmotic performance, the membrane intrinsic transport properties, *A*, *B*, *R*, and *S*, were determined from RO operation and shown in Table 2. The *A* and *R* values of PK-TFC composite were 1.24 L m^{-2} h^{-1} bar^{-1} and 94.1%, respectively. After the deposition of polyamphoteric layer, the PK-TFC-PDA/MPC membrane showed a slightly lower *A* value of 1.07 L m^{-2} h^{-1} bar^{-1} and salt rejection of 95.2%. The lower *B* and higher *R* values of PK-TFC-PDA/MPC membrane are most likely resulted by the denser and more highly-cross-linked PA. Furthermore, the lower water permeability of PK-TFC-PDA/MPC can be ascribed to the presence of the polyamphoteric layer, providing additional permeability barrier, and its higher structural parameter value (209.7 μm), in comparison with PK-TFC membrane (189.5 μm).

Table 2. TFC membrane intrinsic transport properties

Membranes	*A* (L m^{-2} h^{-1} bar^{-1})	*B* (L m^{-2} h^{-1})	*B/A* (bar)	*R* (%)	*S* (μm)
PK-TFC	1.24 ± 0.19	0.38 ± 0.11	0.51	94.1 ± 1.4	189.5
PK-TFC-PDA/MPC	1.07 ± 0.07	0.32 ± 0.08	0.48	95.2 ± 1.9	209.7

The osmotic performance of the TFC membranes was measured in AL-FS mode using 1 M NaCl (draw solution) and Milli-Q water (feed solution). The J_w, J_s, and J_s/J_w values across the TFC membranes were tabulated in Table 3. The PK-TFC-PDA/MPC membrane revealed a slight lower water flux than PK-TFC membrane. Both PK-TFC and PK-TFC-PDA/MPC membranes, however, showed similar salt permeability, consistent with the lower pure water permeability observed during RO testing. The low specific reverse salt flux values of both membranes indicate their high permselectivity.

Table 3. Osmotic performance of the PK-TFC and PK-TFC-PDA/MPC membrane (Membrane orientation: AL-FS; Draw solution: 1.0 M NaCl; Feed solution: Milli-Q water)

Membranes	J_w (L m^{-2} h^{-1})	J_s (g m^{-2} h^{-1})	J_s/J_w (g L^{-1})
PK-TFC	26.9 ± 2.1	3.5 ± 0.3	0.13 ± 0.02
PK-TFC-PDA/MPC	23.7 ± 1.1	4.9 ± 1.3	0.20 ± 0.05

The fouling mitigation capability of the TFC membranes was tested using oily wastewater and BSA as foulants, and the osmotic performance is shown in Fig. 6. In Fig. 6(a), the flux of PK-TFC membrane rapidly reduced at the initial 2 h due to oil layer formation on top of the PA active layer, which prevented water molecule permeation. Finally, the flux reached a stable state with the flux retention of 56% after 10 h filtration. In comparison with PK-TFC membrane, the PK-TFC-PDA/MPC membrane showed a slower flux reduction at the initial time and higher flux retention of 70%. The better anti-oil-fouling characteristic of the PK-TFC-PDA/MPC membrane was mainly a result of the strong water adsorption capacity of the polyamphoteric MPC layer. This allows the formation of a thick water layer around the PA layer, which could easily reject oil layer from the hydrated membrane surface. The fouling experiment results corresponded well with the dynamic anti-oil-adhesion properties. In addition, similarly, the fouling phenomenon for PK-TFC and PK-TFC-PDA/MPC membrane could be observed in Fig. 6(b) when 5000 ppm BSA solution was used as feed. The use of BSA as the model foulant revealed a faster flux decline for the pristine PK-TFC membrane. The J_w of the PK-TFC membrane instantly dropped to 80% of its original water flux, and further dropped to 63% after an hour of operation, which became its final water flux for the rest of the 10 h FO operation. The PK-TFC-PDA/MPC membrane, on the other hand, exhibited a less steep flux decline. After 200 min FO operation with 5000 ppm BSA solution, the membrane with polyamphoteric layer showed high

tolerance against protein fouling, with a flux decline of 25%, significantly lower than that of the PK-TFC membrane sample.

In practical application with real wastewater, the concentration of foulants are usually variable, thus the high concentration of model foulants used in this study were chosen to show that regardless the foulant concentration, the modified membranes would exhibit outstanding fouling resistance with little change in water permeability. The decrease in water permeability due to the membrane modification could be considered marginal (around 10% decrease); however, the fouling resistance results show that without the modification step with the polyampholyte layer, the membrane would immediately drop to 60% of the original water flux within one hour of operation. Therefore, the modification step to introduce the polyampholyte layer on top of the polyamide active layer was worth for potential practical applications of the membrane. These results show the comprehensive anti-fouling properties of PK-TFC-PDA/MPC membrane, making it possible for application in oily emulsion and other types of wastewater.

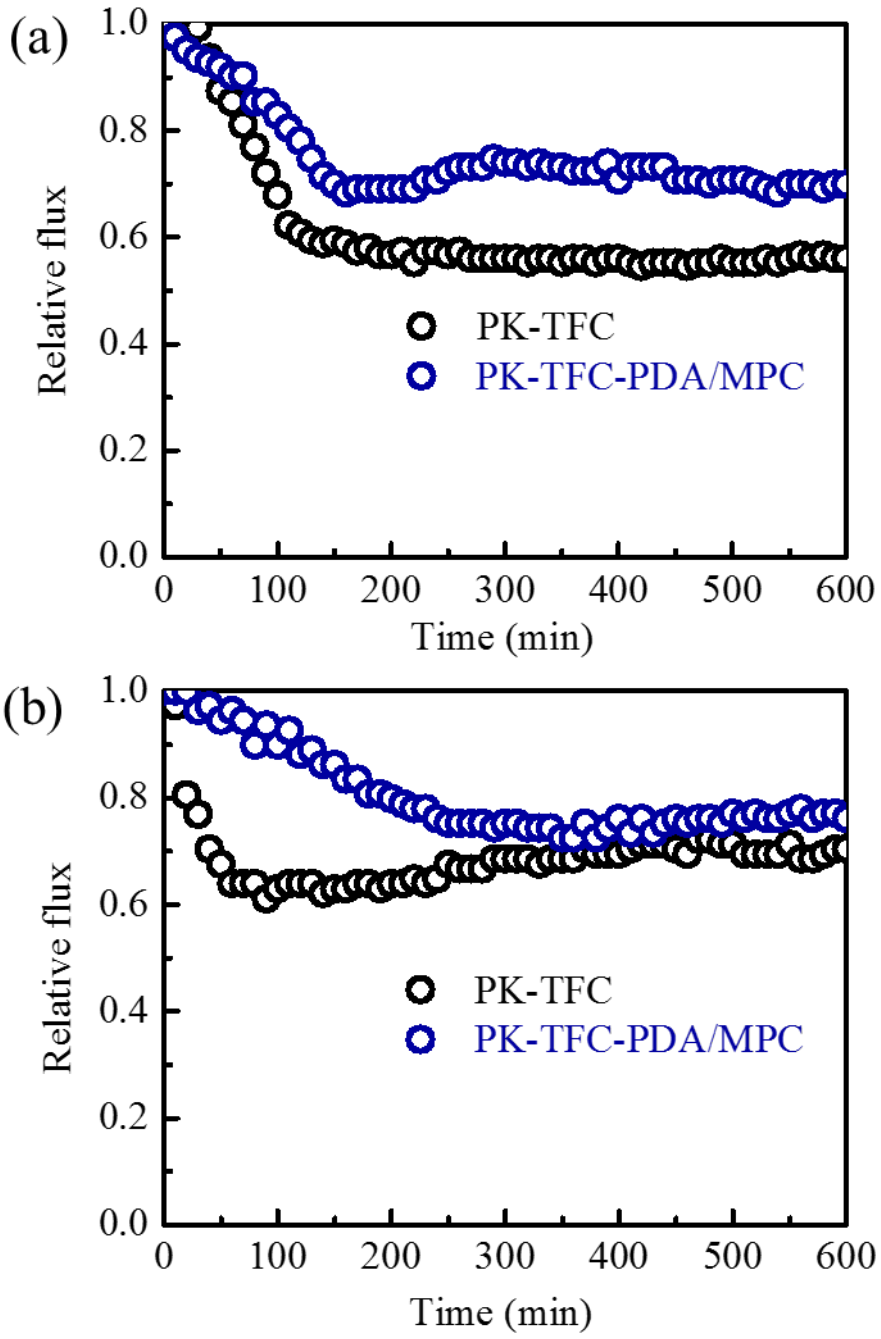

Fig. 6. Anti-fouling performance of the TFC and PK-TFC-PDA/MPC membranes :(a) 10000 ppm soybean oil-in-water emulsion and (b) 5000 ppm BSA solution.

4. Conclusions

A superhydrophilic and superoleophobic TFC FO membrane was prepared by simultaneous deposition of polyamphoteric MPC-co-AEMA and DA, to form an ultrathin mixed layer of PDA and

MPC-co-AEMA atop the TFC PA active layer. The successful immobilization of the polyamphoteric MPC-co-AEMA was mainly due to the adhesive properties of PDA, as well as the covalent interactions with PDA and MPC-co-AEMA. The membrane exhibited a robust superoleophobic characteristic resulting from the polyamphoteric layer's strong water adsorption capacity. In addition, the membrane also exhibited better anti-protein-adhesion property. The FO fouling experiments demonstrated high fouling-resistance properties of PK-TFC-PDA/MPC during treatment of high concentration oily emulsion and protein-containing wastewater.

References

[1] L. Zhang, Y. Lin, H. Wu, L. Cheng, Y. Sun, T. Yasui, Z. Yang, S. Wang, T. Yoshioka, H. Matsuyama, An ultrathin in situ silicification layer developed by an electrostatic attraction force strategy for ultrahigh-performance oil–water emulsion separation, Journal of Materials Chemistry A, 7 (2019) 24569-24582.

[2] D.I. Kim, R.R. Gonzales, P. Dorji, G. Gwak, S. Phuntsho, S. Hong, H. Shon, Efficient recovery of nitrate from municipal wastewater via MCDI using anion-exchange polymer coated electrode embedded with nitrate selective resin, Desalination, 484 (2020) 114425.

[3] J.M. Dickhout, J. Moreno, P. Biesheuvel, L. Boels, R.G. Lammertink, W.M. de Vos, Produced water treatment by membranes: a review from a colloidal perspective, Journal of colloid and interface science, 487 (2017) 523-534.

[4] N. Akther, Y. Lin, S. Wang, S. Phuntsho, Q. Fu, N. Ghaffour, H. Matsuyama, H.K. Shon, In situ ultrathin silica layer formation on polyamide thin-film composite membrane surface for enhanced forward osmosis performances, J. Membr. Sci., (2020) 118876.

[5] M.D. Firouzjaei, S.F. Seyedpour, S.A. Aktij, M. Giagnorio, N. Bazrafshan, A. Mollahosseini, F. Samadi, S. Ahmadalipour, F.D. Firouzjaei, M.R. Esfahani, Recent advances in functionalized polymer membranes for biofouling control and mitigation in forward osmosis, J. Membr. Sci., 596 (2020) 117604.

[6] T. Ni, Q. Ge, Highly hydrophilic thin-film composition forward osmosis (FO) membranes functionalized with aniline sulfonate/bisulfonate for desalination, J. Membr. Sci., 564 (2018) 732-741.

[7] W. Xu, Q. Ge, Novel functionalized forward osmosis (FO) membranes for FO desalination: Improved process performance and fouling resistance, Journal of Membrane Science, 555 (2018) 507-516.

[8] G.T. Gray, J.R. McCutcheon, M. Elimelech, Internal concentration polarization in forward osmosis: Role of membrane orientation, Desalination, 197 (2006) 1-8.

[9] L. Deng, Q. Wang, X. An, Z. Li, Y. Hu, Towards enhanced antifouling and flux performances of thin-film composite forward osmosis membrane via constructing a sandwich-like carbon nanotubes-coated support, Desalination, 479 (2020) 114311.

[10] L. Zhang, Y. Lin, L. Cheng, Z. Yang, H. Matsuyama, A comprehensively fouling-and solvent-resistant aliphatic polyketone membrane for high-flux filtration of difficult oil-in-water micro-and nanoemulsions, J. Membr. Sci., 582 (2019) 48-58.

[11] L. Zhang, L. Cheng, H. Wu, T. Yoshioka, H. Matsuyama, One-step fabrication of robust and anti-oil-fouling aliphatic polyketone composite membranes for sustainable and efficient filtration of oil-in-water emulsions, Journal of Materials Chemistry A, 6 (2018) 24641-24650.

[12] S. Jiang, Z. Cao, Ultralow-fouling, functionalizable, and hydrolyzable zwitterionic materials and their derivatives for biological applications, Adv. Mater., 22 (2010) 920-932.

[13] S. Chen, L. Li, C. Zhao, J. Zheng, Surface hydration: Principles and applications toward low-fouling/nonfouling biomaterials, Polymer, 51 (2010) 5283-5293.

[14] G.V. Dizon, Y.-N. Chou, L.-C. Yeh, A. Venault, J. Huang, Y. Chang, Bio-inert interfaces via biomimetic anchoring of a zwitterionic copolymer on versatile substrates, J. Colloid Interface Sci., 529 (2018) 77-89.

[15] Y. Zhu, W. Xie, F. Zhang, T. Xing, J. Jin, Superhydrophilic in-situ-cross-linked zwitterionic polyelectrolyte/PVDF-blend membrane for highly efficient oil/water emulsion separation, ACS Applied Materials & Interfaces, 9 (2017) 9603-9613.

[16] K. He, H. Duan, G.Y. Chen, X. Liu, W. Yang, D. Wang, Cleaning of oil fouling with water enabled by zwitterionic polyelectrolyte coatings: overcoming the imperative challenge of oil–water separation membranes, ACS nano, 9 (2015) 9188-9198.

[17] S.-Y. Wang, L.-F. Fang, H. Matsuyama, Electrostatic adsorption behavior of zwitterionic copolymers on negatively charged surfaces, Langmuir, 35 (2019) 9152-9160.

[18] C.H. Liu, J. Lee, C. Small, J. Ma, M. Elimelech, Comparison of organic fouling resistance of thin-film composite

membranes modified by hydrophilic silica nanoparticles and zwitterionic polymer brushes, J. Membr. Sci., 544 (2017) 135-142.
[19] X. Zhang, J. Tian, S. Gao, W. Shi, Z. Zhang, F. Cui, S. Zhang, S. Guo, X. Yang, H. Xie, D. Liu, Surface functionalization of TFC FO membranes with zwitterionic polymers: Improvement of antifouling and salt-responsive cleaning properties, Journal of Membrane Science, 544 (2017) 368-377.
[20] X. Zhang, M. Xie, Z. Yang, H.-C. Wu, C. Fang, L. Bai, L.-F. Fang, T. Yoshioka, H. Matsuyama, Antifouling double-skinned forward osmosis membranes by constructing zwitterionic brush-decorated MWCNT ultrathin films, ACS Applied Materials & Interfaces, 11 (2019) 19462-19471.
[21] S.-Y. Wang, L.-F. Fang, H. Matsuyama, Construction of a stable zwitterionic layer on negatively-charged membrane via surface adsorption and cross-linking, Journal of Membrane Science, 597 (2020) 117766.
[22] H. Lee, S.M. Dellatore, W.M. Miller, P.B. Messersmith, Mussel-inspired surface chemistry for multifunctional coatings, Science, 318 (2007) 426-430.
[23] S. Hong, Y.S. Na, S. Choi, I.T. Song, W.Y. Kim, H. Lee, Non-covalent self-assembly and covalent polymerization co-contribute to polydopamine formation, Adv. Funct. Mater., 22 (2012) 4711-4717.
[24] C. Zhang, Y. Ou, W.X. Lei, L.S. Wan, J. Ji, Z.K. Xu, CuSO4/H2O2-induced rapid deposition of polydopamine coatings with high uniformity and enhanced stability, Angew. Chem. Int. Ed., 55 (2016) 3054-3057.
[25] Z.-Y. Xi, Y.-Y. Xu, L.-P. Zhu, Y. Wang, B.-K. Zhu, A facile method of surface modification for hydrophobic polymer membranes based on the adhesive behavior of poly (DOPA) and poly (dopamine), J. Membr. Sci., 327 (2009) 244-253.
[26] C. Zhang, M.-Q. Ma, T.-T. Chen, H. Zhang, D.-F. Hu, B.-H. Wu, J. Ji, Z.-K. Xu, Dopamine-triggered one-step polymerization and codeposition of acrylate monomers for functional coatings, ACS Appl. Mater. Interfaces, 9 (2017) 34356-34366.
[27] G. Zhang, Y. Li, A. Gao, Q. Zhang, J. Cui, S. Zhao, X. Zhan, Y. Yan, Bio-inspired underwater superoleophobic PVDF membranes for highly-efficient simultaneous removal of insoluble emulsified oils and soluble anionic dyes, Chem. Eng. J., 369 (2019) 576-587.
[28] J.-K. Pi, J. Yang, Z.-K. Xu, One-pot mussel-inspiration and silication: A platform for constructing oil-repellent surfaces toward crude oil/water separation, J. Membr. Sci., 601 (2020) 117915.
[29] Q. Zhu, Q. Pan, Mussel-inspired direct immobilization of nanoparticles and application for oil–water separation, ACS nano, 8 (2014) 1402-1409.
[30] L. Zhang, Z. Cui, M. Hu, Y. Mo, S. Li, B. He, J. Li, Preparation of PES/SPSf blend ultrafiltration membranes with high performance via H2O-induced gelation phase separation, J. Membr. Sci., 540 (2017) 136-145.
[31] L. Zhang, R. Takagi, S. Wang, Y. Lin, K. Guan, L. Cheng, H. Matsuyama, In situ formation of ultrathin polyampholyte layer on porous polyketone membrane via a one-step dopamine co-deposition strategy for oil/water separation with ultralow fouling, Journal of Membrane Science, 619 (2021) 118789.
[32] L. Zhang, Y. Lin, S. Wang, L. Cheng, H. Matsuyama, Engineering of ultrafine polydopamine nanoparticles in-situ assembling on polyketone substrate for highly-efficient oil-water emulsions separation, Journal of Membrane Science, 613 (2020) 118501.
[33] S.-Y. Wang, L.-F. Fang, L. Cheng, S. Jeon, N. Kato, H. Matsuyama, Novel ultrafiltration membranes with excellent antifouling properties and chlorine resistance using a poly (vinyl chloride)-based copolymer, J. Membr. Sci., 549 (2018) 101-110.
[34] R.R. Gonzales, L. Zhang, Y. Sasaki, W. Kushida, H. Matsuyama, H.K. Shon, Facile development of comprehensively fouling-resistant reduced polyketone-based thin film composite forward osmosis membrane for treatment of oily wastewater, Journal of Membrane Science, 626 (2021) 119185.
[35] R.R. Gonzales, Y. Yang, M.J. Park, T.-H. Bae, A. Abdel-Wahab, S. Phuntsho, H.K. Shon, Enhanced water permeability and osmotic power generation with sulfonate-functionalized porous polymer-incorporated thin film nanocomposite membranes, Desalination, 496 (2020) 114756-114765.

[36] Z. Yang, R. Takagi, X. Zhang, T. Yasui, L. Zhang, H. Matsuyama, Engineering a dual-functional sulfonated polyelectrolyte-silver nanoparticle complex on a polyamide reverse osmosis membrane for robust biofouling mitigation, J. Membr. Sci., 618 118757.
[37] R.R. Gonzales, M.J. Park, L. Tijing, D.S. Han, S. Phuntsho, H.K. Shon, Modification of nanofiber support layer for thin film composite forward osmosis membranes via layer-by-layer polyelectrolyte deposition, Membranes, 8 (2018) 70-84.
[38] Y. Sun, Y. Lin, S. Wang, Z. Yang, L. Zhang, H. Matsuyama, Facile modification of aliphatic polyketone-based thin-film composite membrane for three-dimensional and comprehensive antifouling in active-layer-facing-draw-solution mode, J. Appl. Polym. Sci., 138 (2020) 49711.
[39] M.J. Park, R.R. Gonzales, A. Abdel-Wahab, S. Phuntsho, H.K. Shon, Hydrophilic polyvinyl alcohol coating on hydrophobic electrospun nanofiber membrane for high performance thin film composite forward osmosis membrane, Desalination, 426 (2018) 50-59.
[40] R.R. Gonzales, M.J. Park, T.-H. Bae, Y. Yang, A. Abdel-Wahab, S. Phuntsho, H.K. Shon, Melamine-based covalent organic framework-incorporated thin film nanocomposite membrane for enhanced osmotic power generation, Desalination, 459 (2019) 10-19.
[41] F. Volpin, R.R. Gonzales, S. Lim, N. Pathak, S. Phuntsho, H.K. Shon, GreenPRO: A novel fertiliser-driven osmotic power generation process for fertigation, Desalination, 447 (2018) 158-166.
[42] Y. Lv, S.-J. Yang, Y. Du, H.-C. Yang, Z.-K. Xu, Co-deposition kinetics of polydopamine/polyethyleneimine coatings: Effects of solution composition and substrate surface, Langmuir, 34 (2018) 13123-13131.
[43] L.-F. Fang, L. Cheng, S. Jeon, S.-Y. Wang, T. Takahashi, H. Matsuyama, Effect of the supporting layer structures on antifouling properties of forward osmosis membranes in AL-DS mode, J. Membr. Sci., 552 (2018) 265-273.
[44] Z. Yang, D. Saeki, H. Matsuyama, Zwitterionic polymer modification of polyamide reverse-osmosis membranes via surface amination and atom transfer radical polymerization for anti-biofouling, J. Membr. Sci., 550 (2018) 332-339.
[45] S. Karan, Z. Jiang, A.G. Livingston, Sub–10 nm polyamide nanofilms with ultrafast solvent transport for molecular separation, Science, 348 (2015) 1347.
[46] C.Y. Tang, Y.-N. Kwon, J.O. Leckie, Probing the nano-and micro-scales of reverse osmosis membranes—A comprehensive characterization of physiochemical properties of uncoated and coated membranes by XPS, TEM, ATR-FTIR, and streaming potential measurements, J. Membr. Sci., 287 (2007) 146-156.
[47] M.J. Park, C. Wang, D.H. Seo, R.R. Gonzales, H. Matsuyama, H.K. Shon, Inkjet printed single walled carbon nanotube as an interlayer for high performance thin film composite nanofiltration membrane, Journal of Membrane Science, (2020) 118901.
[48] L. Cheng, A.R. Shaikh, L.-F. Fang, S. Jeon, C.-J. Liu, L. Zhang, H.-C. Wu, D.-M. Wang, H. Matsuyama, Fouling-resistant and self-cleaning aliphatic polyketone membrane for sustainable oil–water emulsion separation, ACS Appl. Mater. Interfaces, 10 (2018) 44880-44889.
[49] C.Y. Tang, Y.-N. Kwon, J.O. Leckie, Effect of membrane chemistry and coating layer on physiochemical properties of thin film composite polyamide RO and NF membranes: I. FTIR and XPS characterization of polyamide and coating layer chemistry, Desalination, 242 (2009) 149-167.
[50] B. Barthe´le´my, S. Maheux, S.b. Devillers, F.d.r. Kanoufi, C. Combellas, J. Delhalle, Z. Mekhalif, Synergistic effect on corrosion resistance of Phynox substrates grafted with surface-initiated ATRP (co) polymerization of 2-methacryloyloxyethyl phosphorylcholine (MPC) and 2-hydroxyethyl methacrylate (HEMA), ACS Appl. Mater. Interfaces, 6 (2014) 10060-10071.
[51] Y. Zhu, J. Wang, F. Zhang, S. Gao, A. Wang, W. Fang, J. Jin, Zwitterionic nanohydrogel grafted PVDF membranes with comprehensive antifouling property and superior cycle stability for oil-in-water emulsion separation, Adv. Funct. Mater., 28 (2018) 1804121.

[52] N. Helali, M. Rastgar, M. Farhad Ismail, M. Sadrzadeh, Development of underwater superoleophobic polyamide-imide (PAI) microfiltration membranes for oil/water emulsion separation, Separation and Purification Technology, 238 (2020) 116451.
[53] M.F. Ismail, B. Khorshidi, M. Sadrzadeh, New insights into the impact of nanoscale surface heterogeneity on the wettability of polymeric membranes, Journal of Membrane Science, 590 (2019) 117270.
[54] L. Cheng, D.-M. Wang, A.R. Shaikh, L.-F. Fang, S. Jeon, D. Saeki, L. Zhang, C.-J. Liu, H. Matsuyama, Dual superlyophobic aliphatic polyketone membranes for highly efficient emulsified oil–water separation: performance and mechanism, ACS Appl. Mater. Interfaces, 10 (2018) 30860-30870.
[55] S. Gao, J. Sun, P. Liu, F. Zhang, W. Zhang, S. Yuan, J. Li, J. Jin, A robust polyionized hydrogel with an unprecedented underwater anti-crude-oil-adhesion property, Adv. Mater., 28 (2016) 5307-5314.
[56] W.S. Ang, M. Elimelech, Protein (BSA) fouling of reverse osmosis membranes: Implications for wastewater reclamation, Journal of Membrane Science, 296 (2007) 83-92.
[57] M.-Y. Zhou, P. Zhang, L.-F. Fang, B.-K. Zhu, J.-L. Wang, J.-H. Chen, H. Abdallah, A positively charged tight UF membrane and its properties for removing trace metal cations via electrostatic repulsion mechanism, Journal of Hazardous Materials, 373 (2019) 168-175.